Geophysical Research Letters

RESEARCH LETTER
10.1029/2024GL108645

Electron Energization With Bursty Bulk Flows: MHD With Embedded Particle-In-Cell Simulation

Xiantong Wang[1], Shasha Zou[1], Zihan Wang[2], Weijie Sun[3], Yuxi Chen[4], and Gábor Tóth[1]

[1]Department of Climate and Space Sciences and Engineering, University of Michigan, Ann Arbor, MI, USA, [2]Department of Physics, University of Texas at Arlington, Arlington, TX, USA, [3]Space Sciences Laboratory, University of California, Berkeley, CA, USA, [4]Center for Space Physics and Department of Astronomy, Boston University, Boston, MA, USA

Key Points:

- For the first time, we simulate the bursty bulk flow (BBF) events with kinetic physics embedded in a global magnetosphere model
- The electron velocity distribution functions exhibit different anisotropy features at different locations of the BBF
- Energy dependent electron pitch angle distribution evolutions are identified in the simulation

Correspondence to:
X. Wang,
xtwang@umich.edu

Citation:
Wang, X., Zou, S., Wang, Z., Sun, W., Chen, Y., & Tóth, G. (2024). Electron energization with bursty bulk flows: MHD with embedded particle-in-cell simulation. *Geophysical Research Letters*, *51*, e2024GL108645. https://doi.org/10.1029/2024GL108645

Received 7 FEB 2024
Accepted 26 MAY 2024

Author Contributions:
Conceptualization: Shasha Zou, Zihan Wang, Weijie Sun
Funding acquisition: Shasha Zou
Investigation: Zihan Wang, Weijie Sun
Methodology: Yuxi Chen, Gábor Tóth
Project administration: Shasha Zou
Software: Yuxi Chen, Gábor Tóth
Supervision: Shasha Zou
Writing – review & editing: Shasha Zou, Zihan Wang, Weijie Sun, Yuxi Chen, Gábor Tóth

Abstract Using a two-way coupled magnetohydrodynamics with embedded kinetic physics model, we perform a substorm event simulation to study electron velocity distribution functions (VDFs) evolution associated with Bursty Bulk Flows (BBFs). The substorm was observed by Magnetospheric Multiscale satellite on 16 May 2017. The simulated BBF macroscopic characteristics and electron VDFs agree well with observations. The VDFs from the BBF tail to its dipolarization front (DF) during its earthward propagation are revealed and they show clear energization and heating. The electron pitch angle distributions (PADs) at the DF are also tracked, which show interesting energy dependent features. Lower energy electrons develop a "two-hump" PAD while the higher energy ones show persist "pancake" distribution. Our study reveals for the first time the evolution of electron VDFs as a BBF moves earthward using a two-way coupled global and kinetic model, and provides valuable contextual understanding for the interpretation of satellite observations.

Plain Language Summary Bursty bulk flows (BBFs) are identified as the fast earthward-propagating flows from magnetic reconnection in the Earth's magnetotail. BBFs are related to particle energization and heating processes as reported by satellite observations. For the first time, we use a novel numerical model that simulates kinetic physics directly in a global model. The electron velocity distribution functions extracted from multiple locations associated with BBF show good agreements with the satellite in situ observations. The energization and heating of the electrons associated with BBF and their energy-dependent pitch angle distributions are revealed.

1. Introduction

Initially observed by Baumjohann et al. (1990) and later further demonstrated by Angelopoulos et al. (1992, 1994) using AMPTE satellite data, bursty bulk flows (BBFs) are characterized by their transient (~10-min) fast (~400 km/s) plasma flow enhancement in the magnetotail. The concurrent B_z increase is identified at the dipolarization fronts (DFs) during BBFs (Fu et al., 2012; Nakamura et al., 2002; Runov et al., 2009). Consequently, BBFs serve as an efficient mechanism for transporting magnetic flux from the magnetotail to the inner magnetosphere (Angelopoulos et al., 2013; Huang et al., 2015; Nakamura et al., 2009). Furthermore, BBFs are associated with plasma phenomena, such as plasma wave activities, energetic particles injection into the inner magnetosphere, and field-aligned currents and particle precipitations into the ionosphere (Angelopoulos et al., 1996, 1997; Gabrielse et al., 2014; Henderson et al., 1998).

Numerical simulations have played a pivotal role in the study of BBFs within the magnetotail over the past several decades. Birn et al. (1996) utilized regional magnetohydrodynamic (MHD) simulations to demonstrate the connection between the plasmoid formation and dipolarization in the inner magnetosphere. In subsequent simulation work by Birn et al. (2004), the authors discovered that the reduction of the flux tube entropy is facilitating the earthward propagation of the BBFs. In addition to the regional MHD simulations for the magnetotail, the development of global MHD models enables the study of the BBFs in a more realist setup. Employing the Lyon-Fedder-Mobarry (LFM) global MHD magnetosphere model (Lyon et al., 2004), Wiltberger et al. (2000) simulated several fast flow channels in the magnetotail during an isolated subtorm, and the plasma and magnetic field properties showed good agreement with the observation reported by Angelopoulos et al. (1992). The OpenGGCM model (Raeder et al., 2008) was also used by Ge et al. (2011) to study the propagation of the dipolarization front and they concluded the causality between the auroral breakup represented by the simulated energy flux in the simulation and the flow vortices formed around the BBF flows. Recent investigations using

numerical simulation have further advanced the understanding of BBF events. Wiltberger et al. (2015) conducted a high-resolution global MHD simulation with the LFM model to study the BBF behavior under steady southward IMF conditions. The authors confirmed that BBFs are driven by the onset of new reconnection and its related fast earthward flows. Superposed epoch analysis was also conducted, and the overall plasma and magnetic field properties were found to be similar to the observations although with differences in plasma density profiles near the BBFs (Wiltberger et al., 2015).

Despite the progress made with regional and global MHD simulations on the general properties of the BBF events as described above, there is a need to simulate BBFs with kinetic models to investigate the particle velocity distribution evolution and energization processes. First, the acceleration near the neutral line at the site of reconnection was investigated. In these studies, energetic electrons up to approximately 300 keV near the center of the diffusion region were observed by the Wind spacecraft (Øieroset et al., 2002). The energization mechanism of these relativistic electrons were later examined by regional particle-in-cell simulations. The electrons with velocity component $V_x \sim 0$ at the X line are accelerated across the tail by the inductive reconnection electric field E_y (Hoshino, 2005; Pritchett, 2006). Subsequently, betatron acceleration related to the magnetic field dipolarization when the plasma flow propagates toward Earth was studied to explain the electron acceleration signature during substorms (Asano et al., 2010; Baker et al., 1982; Birn et al., 1998). Meanwhile, the energization mechanism of ions was also studied by observations and simulations. Using THEMIS observations, X.-Z. Zhou et al. (2010) noticed that energetic ions exist ahead of the DF, which was later explained by precursor flow formed by ion reflections using test-particle simulation (X.-Z. Zhou et al., 2011). This argument is also supported by implicit PIC simulations (Eastwood et al., 2015). This ion reflection also exists in tailward DFs from ARTEMIS observations (X.-Z. Zhou et al., 2015). Similar to electrons, Betatron and Fermi accelerations are also found to account for ion energization (Lu et al., 2016; Runov et al., 2015; Xu et al., 2019; X.-Z. Zhou, Tóth, et al., 2019). In addition to velocity distribution functions, understanding the particle pitch angle distribution (PAD), especially the electron PAD, is crucial for comprehending particle energization associated with BBFs. Various electron PADs have been observed in the wake of DFs. Among them, the pancake distribution (electron pitch angle primarily at 90°) has been reported within the evolving Flux Pileup Regions (FPRs) (Fu et al., 2011; C. Liu et al., 2017) near the neutral sheet, and it is recognized as being associated with the betatron acceleration mechanism (Fu et al., 2011). However, the detailed information regarding when and where particles become energized and how their velocity or pitch angle distribution functions are altered while the BBF structure evolves remains an open question.

Currently, MHD models are unable to capture the kinetic physics of the plasma, and the PIC simulations mentioned earlier are limited to regional simulations without a global magnetosphere configuration. As a result, there remains a significant gap in the literature regarding self-consistent simulations that couple global MHD and localized PIC models to investigate the evolution of BBF events. In this paper, we will use the two-way coupled MHD and PIC modeling approach to fill in this gap. A substorm event on 16 May 2017 is simulated by the BATSRUS MHD model with local kinetic physics captured by the FLEKS PIC code. This two-way coupled model allows the investigation of the evolution of electron velocity distributions and the subsequent formation of anisotropy at various locations of the BBF. The pitch angle distributions of the electrons can also be examined to provide insights into the field-aligned current generation process.

The model description and simulation setup are described in Section 2, the simulation results are presented in Section 3 and we conclude in Section 4.

2. Simulation Setup

We use MHD with embedded PIC (MHD-EPIC) model (Chen & Tóth, 2019; Daldorff et al., 2014) to simulate Earth's magnetosphere. In MHD-EPIC, the BATS-R-US MHD code (Powell et al., 1999; Tóth et al., 2008) and semi-implicit particle-in-cell (PIC) code FLEKS (Chen et al., 2023) are two-way coupled through SWMF (Gombosi et al., 2021; Tóth et al., 2012). A three-dimensional block-adaptive Cartesian grid of BATS-R-US is used to cover the entire computational domain: $-224\ R_E < x < 32\ R_E$ and $-128\ R_E < y, z < 128\ R_E$ in GSM coordinates. The semi-relativistic ideal MHD with electron pressure equations are solved in most of the simulation domain. The PIC model is solved in a box region with a spherical cut out. The box is in the magnetotail ($-60\ R_E < x < 0$ and $-12\ R_E < y, z < 12\ R_E$) from which the sphere with radius $r = 10\ R_E$ centered around Earth is excluded to avoid overlap with the Rice Convection Model (RCM) (Toffoletto et al., 2003; Wolf et al., 1982)

simulating the inner-magnetosphere. Moreover, we solve the Hall MHD equations around the PIC region ($-100\ R_E < x < 0$, $-30\ R_E < y < 30\ R_E$, and $-20\ R_E < z < 20\ R_E$ excluding a sphere with radius $r = 3\ R_E$ centered around Earth) to achieve more consistent coupling. The grid resolution is set to 1/8 R_E for both the PIC and MHD models in the PIC region. The ionospheric electrodynamics is simulated by the Ridley Ionosphere Model (RIM) (Ridley et al., 2004), which solves a Poisson-type equation for the electric potential on a 2-D spherical grid with a $1° \times 1°$ grid resolution. The presented simulation setup was applied to study geomagnetic storm by Wang et al. (2022a). Moreover, the MHD-EPIC model has been applied to studying several planetary and moon magnetospheres, including Mercury (Chen et al., 2019; Li et al., 2023), Earth (Chen et al., 2017, 2020; Wang et al., 2022b), Mars (Ma et al., 2018), and Ganymede (Tóth et al., 2016; H. Zhou, Tóth, et al., 2019, 2020).

In PIC simulations, reduced speed of light c and ion-electron mass ratio m_i/m_e are often used to make the simulation feasible to the computational resources (Daughton et al., 2011; Lapenta et al., 2010; Y.-H. Liu et al., 2014). In the presented simulation, $c = 10{,}000$ km/s to accelerate the convergence of the implicit electric field solver, and $m_i/m_e = 100$ to increase the electron kinetic scale. The ion and electron masses per charge are also increased by a factor of 16 to increase the kinetic scales (ion inertial length and electron skin depth) so that they can be resolved with an affordable grid resolution. Tóth et al. (2017) concludes that by introducing this scaling factor 16, (a) the solution of the equations is not sensitive to the scaling at global scales, and (b) the solutions at the kinetic scale, such as the width of the ion diffusion region and the overall structures of the reconnection jets, are proportional to the scaling factor but otherwise remain the same. In our simulation, the ion inertial length in most areas of the magnetotail is larger than 1 R_E with the scaling factor applied, which can be well resolved by the 1/8 R_E grid resolution. The electron skin depth is 10 times smaller, which is only marginally resolved, but the solution overall remains valid at the resolved scales (Chen & Tóth, 2019).

We apply the MHD-EPIC model to the substorm event on 16 May 2017 from 11:00:00 to 15:00:00 UT. Panel 1(a) shows the 3-D overview of the simulation domain at T = 13:30:00 UT from the simulation presented in this paper. The gray isosurface marks the simulation domain that is covered by the kinetic model while the rest of the simulation domain is simulated using MHD. The color contour in panel (a) is the plasma bulk velocity in the x direction on the equatorial plane, and the semi-transparent box shows the region where the PIC model is applied. The $r = 3\ R_E$ body is also visualized colored with the radial component of the current density j_r. A closer look at the $r = 3\ R_E$ body is placed at the lower right corner. First, the BATS-R-US and RIM models are run to reach a quasi-steady state under the solar wind condition at 11:00:00 using local time stepping with 2,500 iterations. Next, the FLEKS and RCM models are switched on and the SWMF is run in time-accurate mode. The most relevant solar wind parameters, including the solar wind density ρ, velocity V_x and IMF B_z, are plotted in Panel 1(c), suggesting moderate driving condition. This substorm was observed in the auroral electrojet index (AE), presented in Panel 1(c), and also by individual ground magnetometers near Alaska (not shown). The MMS observations also captured the loading and the subsequent unloading processes, which initiated at 13:21 UT. The subtorm onset based on the AE index is later than the MMS observation and at about 13:42 UT.

3. Results

3.1. Overview of the Substorm

Throughout the simulated event, the MMS1 satellite traversed the dawn side of the magnetotail with an averaged location at $(-14.23, -8.99, 0.37)\ R_E$ in GSM coordinates. As depicted in Figure 1b, we present the profiles of the total magnetic field strength (B_t), its x and z components, and the x component of the plasma bulk velocity in GSM coordinates from MMS measurements (in black) and the simulation outputs (in red). The persistently negative x component of the magnetic field shows that the virtual satellite position is on the same side as the MMS satellite in the tail current sheet. From the MMS observation, loading and unloading processes can be seen clearly in the variation of the total magnetic field strength. The decline of B_t commenced around 13:20 UT and signaled the unloading process. This trend is not captured by the MHD-EPIC model, because the simulated magnetotail is constantly volatile in this time range. This can also be observed from the B_z and V_x comparisons. The MMS observation shows a dipolarization between 13:45 UT to 14:00 UT, which is also captured by the MHD-EPIC model. Multiple earthward flows are evident within the ion bulk velocity V_x, attaining maximum speeds exceeding 500 km/s. Although it is difficult to have one to one match for each dipolarization, the overall magnitudes of the B_z and V_x exhibit reasonable agreement between the observation and simulation during the dynamic time in the magnetotail. Illustrated in Figure 1a is the comprehensive layout of the simulation domain, revealing

10.1029/2024GL108645

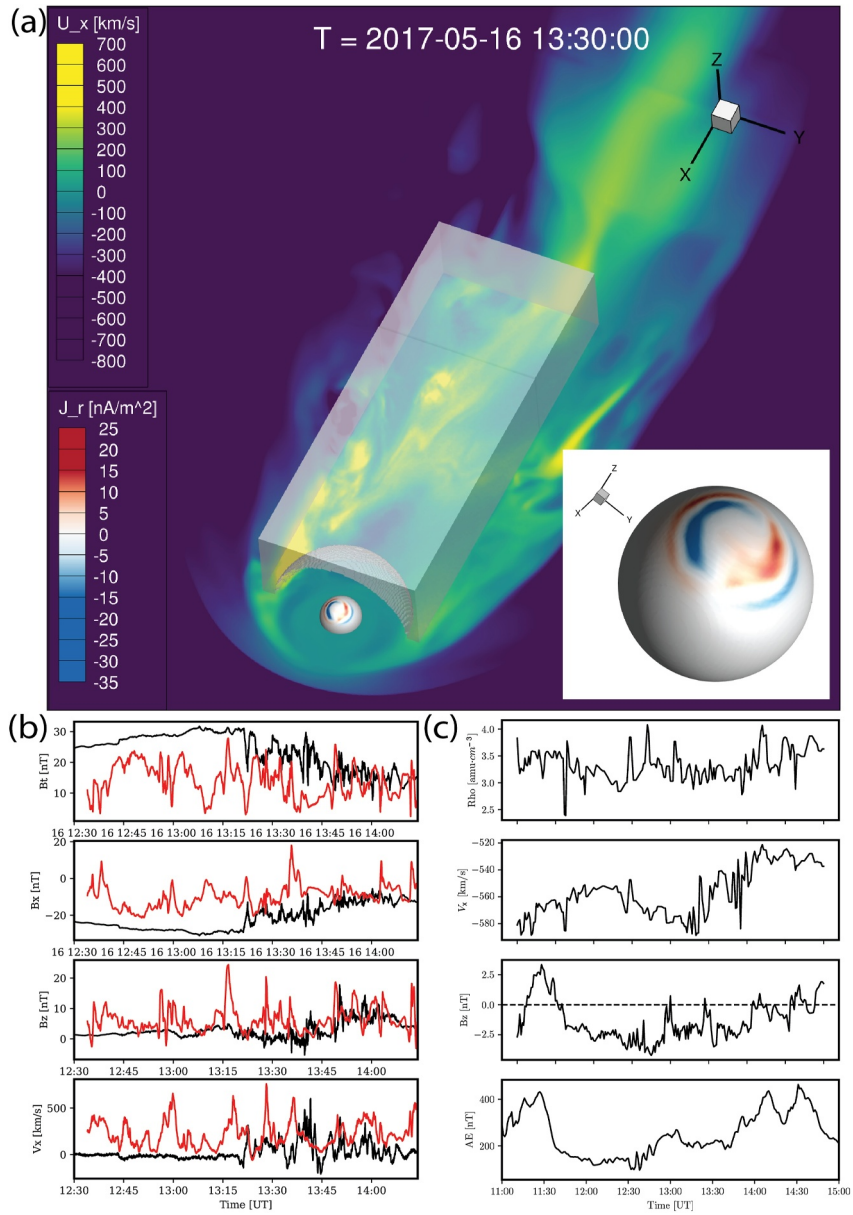

Figure 1. (a) Overview of the simulation domain. The color contour of the x direction of the plasma bulk velocity is plotted on the equatorial plane at 2017-05-16 13:30 UT. The area inside the gray iso-surface is simulated by the PIC model and the rest of the simulation domain is simulated by the MHD model. The radial current is plotted on the $R = 3\ R_E$ surface. (b) Comparison between the simulation output (red) and the MMS observations (black). (c) Key solar wind parameters used as drivers and the observed AE index used to identify the substorm onset.

the ion bulk velocity contour on the equatorial plane, with peak speeds surpassing 700 km/s. Multiple instances of earthward flow injections manifest on the equatorial plane, suggesting that the simulation successfully captures multiple earthward plasma flows with the MHD-EPIC model.

In the following subsections, we will take a closer look at the detailed structure of the BBF and the associated particle velocity distribution functions at multiple locations surrounding the BBF.

3.2. General Properties of the BBF

The observations in Figure 1b show that the magnetotail became more active after $t \approx$ 13:20 UT, when the unloading process initiated. Figure 2a–2d show a four-minute time interval from 13:49 UT to 13:52 UT of a major

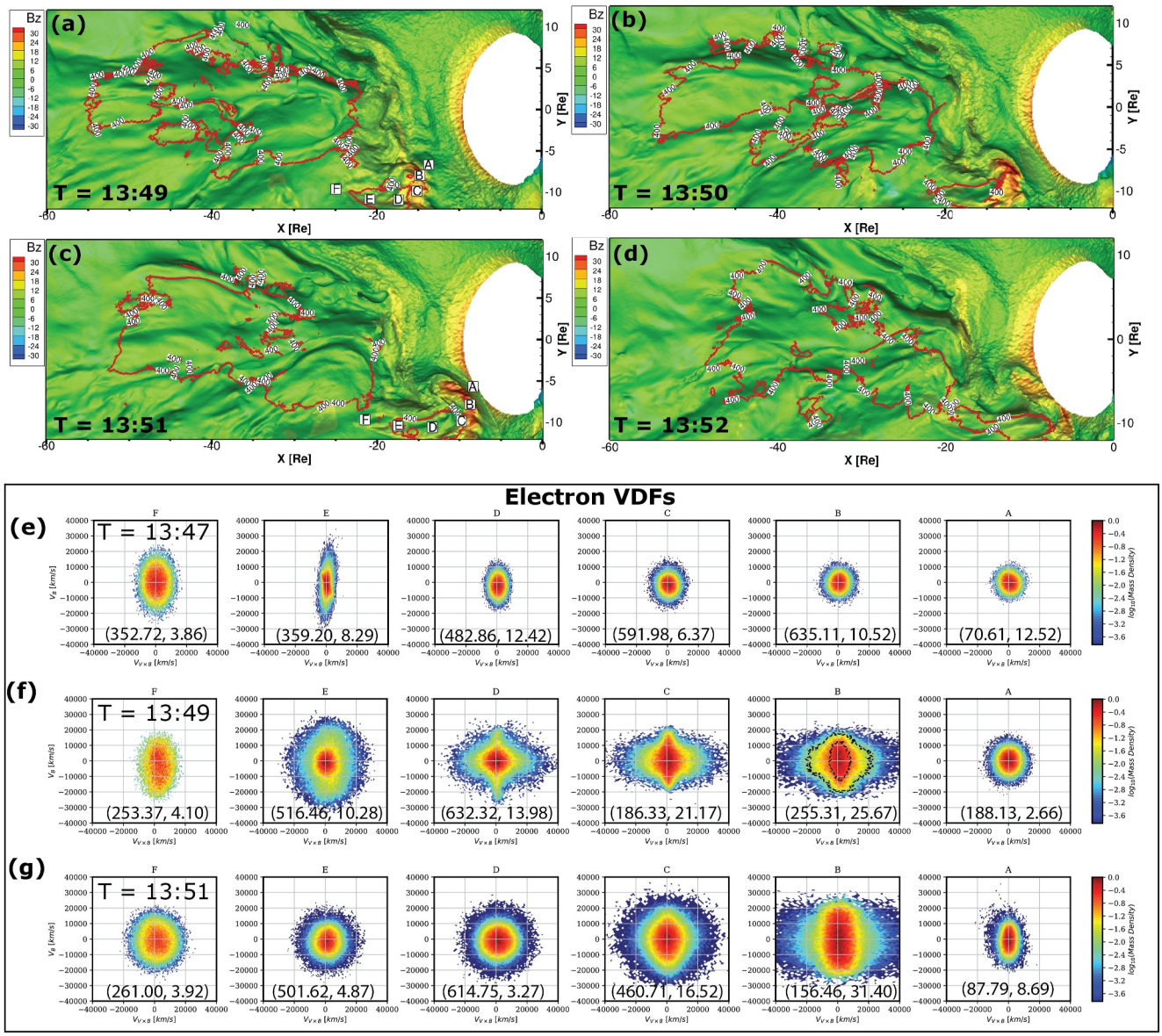

Figure 2. (a)–(d) The $B_x = 0$ iso-surface colored by B_z at four times from 13:49 UT to 13:52 UT. The 400 km/s contour lines of the plasma bulk velocity in the x direction are shown in red. (e)–(f) The electron velocity distribution functions (VDFs) at locations A to F annotated in Panel (a). (g) The electron VDFs at the time and locations A to F annotated in Panel (c). The pair of numbers in parentheses in Panels (e)–(g) show the ion bulk velocity V_{ix} (in km/s) and the magnetic field component B_z (in nT).

simulated BBF event identified by the peak in V_x in Figure 1b, obtained from the simulated PIC region. To analyze the BBF characteristics on the current sheet better, the physical quantities are extracted on the surface where $B_x = 0$. The z component of the magnetic field B_z in GSM coordinate is plotted on the current sheet surface with color in each panel. The red contour lines delineate areas where the earthward ion bulk velocity V_x is larger than 400 km/s. The targeted BBF can be identified as the rapid flow channels propagating toward Earth on the dawn side. At the front of these earthward flow channels, there are enhancements in B_z, that is, dipolarization fronts. The B_z enhancement initiated at $x \approx -20$ R_E and propagated into the inner-magnetosphere in the subsequent minutes. Compared to the background B_z, which is less than 10 nT in most of the magnetotail, at the DF, B_z is enhanced above 30 nT. The simulated azimuthal spatial scale of the BBF flow channel is about 3 R_E at the early stage of the BBF and expanded to $\approx$5 R_E as it propagates closer to Earth, which is comparable to a statistical study using Cluster observations (Nakamura et al., 2004) and MHD simulation results (Ge et al., 2011; Wiltberger et al., 2015).

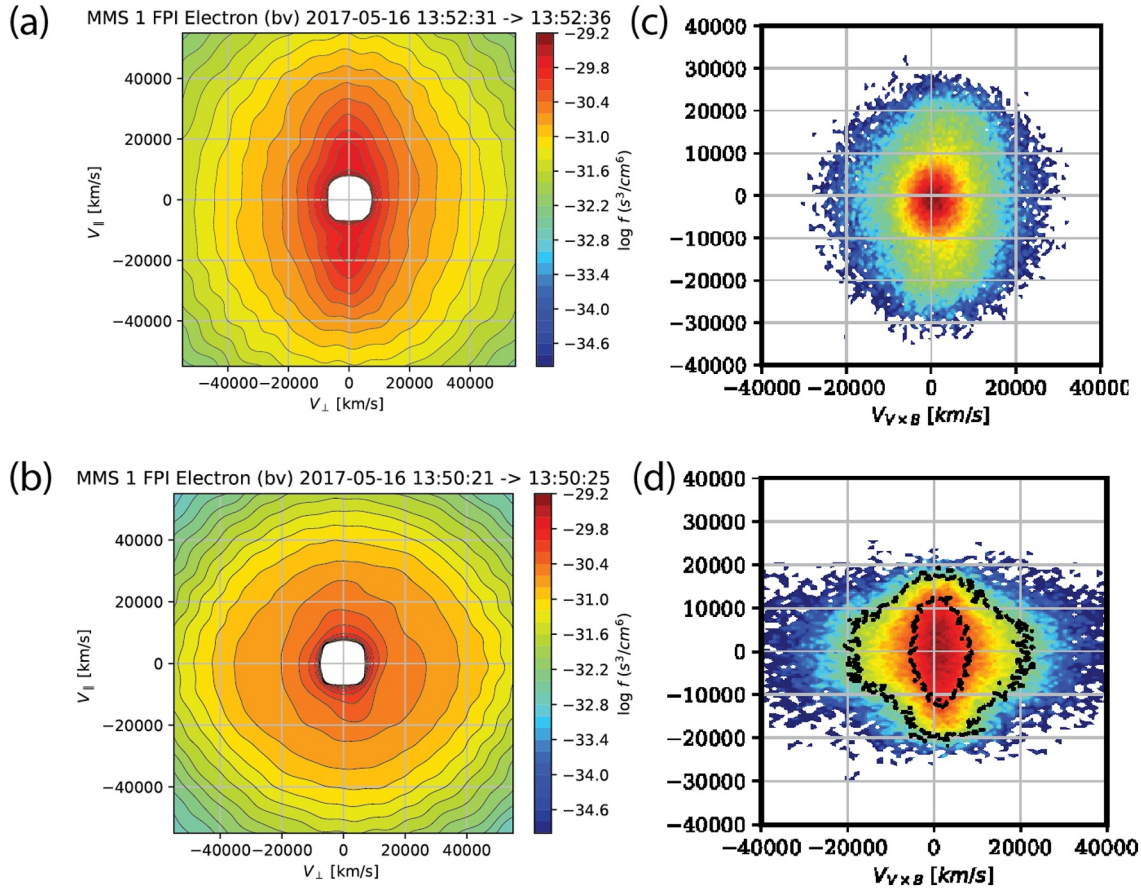

Figure 3. Electron velocity distribution function comparison between MMS (a), (b) and simulation (c), (d). (a)–(b) Electron VDFs at the tailing part of the BBF. (c)–(d) Electron VDFs near the B_z maximum of the BBF.

3.3. Electron Velocity Distribution Functions Evolution Associated With the BBF

To further validate the simulation results, the electron VDFs from the Fast Plasma Investigation (FPI) suite of the MMS satellite (Pollock et al., 2016) are presented in Figure 3 together with the simulation results. Figure 3a is extracted from a location inside the trailing part of the BBF, while Figure 3b is extracted near the B_z maximum of the BBF. The corresponding electron VDFs from the MHD-EPIC model are presented in Figures 3c and 3d, respectively. At the trailing part of the BBF, the electron VDF shows dominantly parallel anisotropy, suggesting that the electrons are experiencing Fermi acceleration. At the leading part of the BBF near the B_z maximum, the high energy electrons are energized favorably in the perpendicular directions, suggesting the betatron acceleration mechanism, while the low energy electrons still exhibit parallel anisotropy. Overall, the agreements between the observed and simulated electron VDFs at the leading and trailing parts of the BBF are very good. The different energization mechanisms at the different locations of BBFs have also been suggested and discussed by Sun et al. (2022).

In situ satellite observations provide valuable information about the electron VDFs at limited locations. The good agreement between simulation and observation gives us the confidence to analyze the simulation results further. To obtain a better picture of the electron velocity distributions over a larger spatial area, in particular the different locations associated with the BBF, six sampling locations, labeled from A to F, have been chosen to extract electron VDFs and are annotated in Panels (a) and (c) of Figure 2. These points were selected based on their relative positions with respect to the general BBF structure, spanning from the far end of the BBF to the immediate location in front of dipolarization front (DF). Specifically, F is positioned just beyond the rear end of the BBF, while E is within the BBF and closer to the rear end. Moving closer to Earth, D marks the location in the middle of the fast flow area. C is situated nearer to the DF, while B precisely coincides with the DF, where the

magnetic field B_z component reaches its maximum. Finally, A is situated ahead of the DF, offering insight into the plasma environment preceding the BBF within the near-Earth plasma sheet. Sampling locations F to A for the VDFs shown in Panels (e) and (f) are annotated in Panel (a), while sampling locations for VDFs shown in Panel (g) are annotated in Panel (c). In Panels (e)–(g), these electron velocity distributions are projected onto the perpendicular (x-axis) and parallel (y-axis) directions relative to the local magnetic field direction. The perpendicular direction follows the orientation of $V \times B$, with V representing the local ion bulk velocity. The local ion bulk velocity has been subtracted from the particle velocities. The local ion bulk velocity and B_z at those sampling locations from three time points are annotated in each panels in Figures 2e–2g.

First, we examine the perturbations due to the incoming BBF by extracting the electron VDFs at the same locations for 13:47 UT (panel e) and 13:49 UT (panel f). The local magnetic field is updated accordingly at each cadence to project the particle velocities onto the coordinate system presented. At locations F and E, electrons exhibit strong velocity anisotropy in the parallel direction, that is, cigar shape, indicating Fermi accelerations. This feature is transient and disappears at location E after 2 min. At locations D to B, by comparing Panel (e) and (f), the electron VDFs expand significantly in both perpendicular and parallel directions from a much colder isotropic distribution 2 min earlier. Thus, the comparison between the VDFs at 13:47 UT and 13:49 UT clearly shows that the propagating BBF can significantly perturb the local electron VDFs. A virtual satellite in the simulation would observe clear plasma energization and heating signals.

Second, we compare and contrast electron VDFs at different locations across the BBF structure at 13:49 UT in panel (f) of Figure 2. At location F, electrons start with parallel anisotropy, due to being in close vicinity of the reconnection site. At location E, the perpendicular energy of electrons is slightly enhanced. Advancing to location D, the perpendicular electron energy is enhanced substantially, altering the VDF to become perpendicularly dominant. This indicates that electrons experience the betatron acceleration mechanism. From location C to B, electrons with different energies show different evolution. Higher energy electrons experience substantial energization in the perpendicular direction influenced by the betatron acceleration mechanism, while electrons at lower energies clearly prefer parallel direction suggesting the dominant role of Fermi acceleration. Moreover, the electrons in front of the DF at location A, barely perturbed, exhibit a significantly lower temperature than those at the DF.

Third, we compare the electron VDFs at similar relative locations of the BBF following the BBF's earthward propagation using Panels (f) and (g). Panel (f) presents the electron VDFs during the early phase of the BBF at 13:49 UT, while the corresponding VDFs at 13:51 UT are illustrated in Panel (g). The BBF DF propagated from about 15 Re to 9 Re within these 2 mins. By comparing the corresponding panels at these two time cadences, one can see that the electron VDFs are more isotropic behind the DF at locations E and D. At locations C and B, which are closer to the further strengthened DF, the electron VDFs show continuing energization and heating. At 13:51 UT, the local B_z enhanced to 31.40 nT at location B from 25.67 nT at 13:49 UT, which results in more prominent betatron acceleration that can be identified from the VDF. The different anisotropy trends for low and high energy electrons persist while the BBF evolves.

3.4. Electron Pitch Angle Distributions Associated With the BBF

We further extracted electrons at the location where B_z reaches its maximum value of the Flux Pileup Region (FPR) from 13:49 UT to 13:51 UT, and present the electron PADs as a function of energy in panels (a1–a3) in Figure 4. The electron PADs exhibit distinct energy-dependent evolutions. Electrons are divided into two energy groups: low ($0.5 - 2.2$ keV) and high energy (>2.2 keV). At 13:49 UT, when the peak FPR is at around $-14.8\ R_E$, high-energy electrons display a pancake PAD in Panel (b2). As the FPR propagates closer to Earth at $-11.9\ R_E$ at 13:50 UT and at $-8.4\ R_E$ at 13:51 UT, the pancake PAD for the high-energy electrons remains prominent, as evident in Panel (b2). However, within these 2 minutes, the PAD peak flattens and the distribution becomes slightly more isotropic. On the other hand, in Panel (b1), the low energy electrons PAD transitions from a pancake-like PAD to a butterfly distribution with maxima around 25° and 155°. This is likely a signature that the Fermi acceleration mechanism plays a more important role for electrons in this energy range. The specificity of the electron PAD over energy bands was also discovered by a THEMIS-D observation reported in Runov et al. (2012, Figure 9g): PAD of the higher energy band shows enhancement near 90° electron flux while the lower energy band exhibits a "two-hump" distribution.

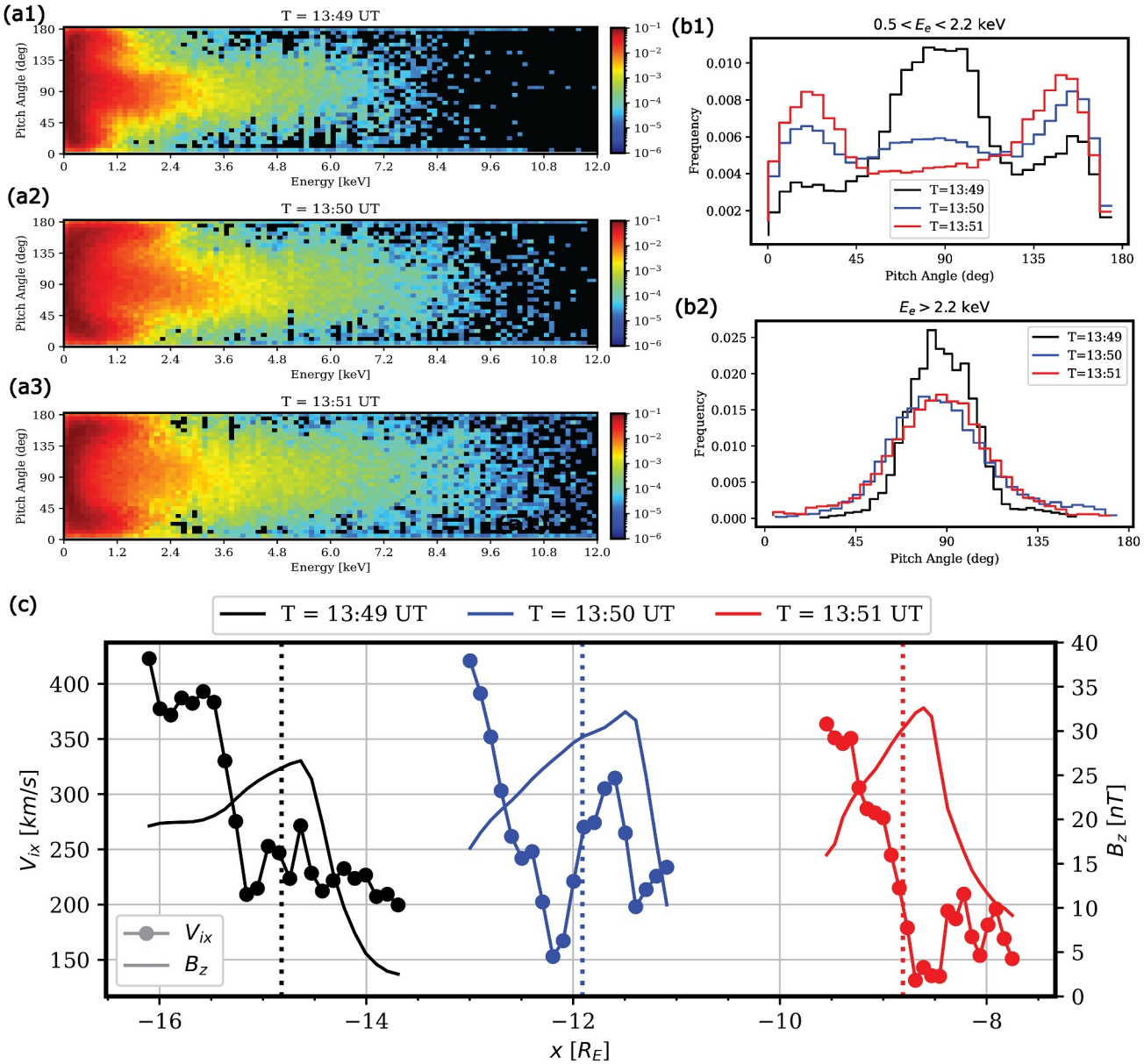

Figure 4. The pitch angle distribution functions from the B_z maximum at t = 13:49 UT, t = 13:50 UT and t = 13:51 UT. (a1)–(a3) The electron pitch angle distributions with regard to electron energy. (b1)–(b2) The pitch angle distributions for low energy (0.5–2.2 keV) and high energy (>2.2 keV) electrons. (c) The ion bulk velocity and B_z profiles for the presented FPR at three different times.

In Figure 4c, we illustrate the ion bulk velocity and B_z profiles of the FPR for the same period. Vertical lines indicate the locations where particles were extracted for the above pitch angle analysis. The compression of the magnetic field is evident from the increased B_z peak from ∼27 nT to ∼33 nT, and reduced spatial extension along the x direction. All B_z peaks are located in front of a steep BBF flow speed reduction region. The 22% increase of the peak B_z intensity is consistent with the increase of the maximum electron energy (from ∼6.6 keV to ∼8 keV, 23%), suggesting that the increase of the electron energy observed from Panel (a1) to (a3) is likely due to the betatron mechanism.

4. Summary and Conclusions

In this paper, we use the two-way coupled MHD-EPIC model to study the spatial and temporal evolutions of the electron VDFs associated with BBFs during substorms. The substorm event occurred at about 13:42 UT on 16

May 2017, and the simulation was conducted from 11:00 UT to 15:00 UT with the target BBF event occurred from 13:49 UT to 13:52 UT. The peak BBF flow speed exceeded 600 km/s. Different from prior simulation studies on BBF events, the magnetotail dynamics in this study is simulated using the PIC model to capture kinetic physics, while the global magnetospheric configuration is simulated by the global MHD model. Therefore, the kinetic physics of the magnetotail is simulated with a more realistic initial and boundary conditions throughout the substorm event.

We compare the magnetic field and plasma properties at the extracted virtual satellite locations with those from the MMS satellite. The comparison yields good agreement, which indicates that the overall magnetosphere configuration is well reproduced by the MHD-EPIC model. The azimuthal(radial) spatial scale of the simulated BBF is about 3 R_E (0.5 R_E). The magnetic field component B_z at the DF exceeds 30 nT. All of those BBF characteristics agree well with statistical results. Therefore, the morphological features of the BBF are well reproduced by the MHD-EPIC model.

To demonstrate the kinetic features associated with BBFs, the electron VDFs and PADs are analyzed. The comparisons between the simulated and observedVDFs are satisfactory, suggesting the high fidelity of the PIC model. We compare the electron VDFs at the same locations before and after the BBF arrival to reveal its impact. Initially cold and isotropic, the electron distributions show significant energization and heating in both perpendicular and parallel directions after its arrival. The VDFs at different locations inside the BBF observed simultaneously reveal a clear trend from more field-aligned near the tail of the BBF to more perpendicular at its front. We also compare the VDFs at different locations relative to the BBF, while it propagates. Near its tail, the VDFs became more isotropic, while those near the DF continuously energized and heated in both perpendicular and parallel directions. The electron PAD evolutions near FPR depend on their energies. For low energy electrons, "two-hump" distribution peaking at 25 and 155° developed from an initial pancake distribution, while for high energy electrons, the pancake distribution persisted.

In the future, we aim to conduct further investigations about the source of the energized electrons and quantifying the different energization processes using the two-way coupled MHD-EPIC model with particle tracking feature included.

Data Availability Statement

Data is available at (Wang, 2024) SWMF software (SWMF-Team, 2024) MMS data (Angelopoulos et al., 2019).

Acknowledgments
This work was supported by NASA 80NSSC20K1313 and NSFAGS-2349872. G. Toth is supported by NSF PRE-EVENTS Grant 1663800. Weijie Sun is supported by NASA 80NSSC24K0069 and 80NSSC24K0452. HPC resources are from NASA Pleiades supercomputer.

References

Angelopoulos, V., Baumjohann, W., Kennel, C., Coroniti, F. V., Kivelson, M., Pellat, R., et al. (1992). Bursty bulk flows in the inner central plasma sheet. *Journal of Geophysical Research*, *97*(A4), 4027–4039. https://doi.org/10.1029/91ja02701

Angelopoulos, V., Coroniti, F., Kennel, C., Kivelson, M., Walker, R., Russell, C., et al. (1996). Multipoint analysis of a bursty bulk flow event on April 11, 1985. *Journal of Geophysical Research*, *101*(A3), 4967–4989. https://doi.org/10.1029/95ja02722

Angelopoulos, V., Cruce, P., Drozdov, A., Grimes, E., Hatzigeorgiu, N., King, D., et al. (2019). The space physics environment data analysis system (SPEDAS). *Space Science Reviews*, *215*, 1–46. https://doi.org/10.1007/s11214-018-0576-4

Angelopoulos, V., Kennel, C. F., Coroniti, F. V., Pellat, R., Kivelson, M. G., Walker, R. J., et al. (1994). Statistical characteristics of bursty bulk flow events. *Journal of Geophysical Research*, *99*(A11), 21257–21280. https://doi.org/10.1029/94ja01263

Angelopoulos, V., Phan, T., Larson, D., Mozer, F., Lin, R., Tsuruda, K., et al. (1997). Magnetotail flow bursts: Association to global magnetospheric circulation, relationship to ionospheric activity and direct evidence for localization. *Geophysical Research Letters*, *24*(18), 2271–2274. https://doi.org/10.1029/97gl02355

Angelopoulos, V., Runov, A., Zhou, X.-Z., Turner, D., Kiehas, S., Li, S.-S., & Shinohara, I. (2013). Electromagnetic energy conversion at reconnection fronts. *Science*, *341*(6153), 1478–1482. https://doi.org/10.1126/science.1236992

Asano, Y., Shinohara, I., Retinò, A., Daly, P., Kronberg, E., Takada, T., et al. (2010). Electron acceleration signatures in the magnetotail associated with substorms. *Journal of Geophysical Research*, *115*(A5). https://doi.org/10.1029/2009ja014587

Baker, D., Fritz, T., Wilken, B., Higbie, P., Kaye, S., Kivelson, M., et al. (1982). Observation and modeling of energetic particles at synchronous orbit on July 29, 1977. *Journal of Geophysical Research*, *87*(A8), 5917–5932. https://doi.org/10.1029/ja087ia08p05917

Baumjohann, W., Paschmann, G., & Lühr, H. (1990). Characteristics of high-speed ion flows in the plasma sheet. *Journal of Geophysical Research*, *95*(A4), 3801–3809.

Birn, J., Hesse, M., & Schindler, K. (1996). MHD simulations of magnetotail dynamics. *Journal of Geophysical Research*, *101*(A6), 12939–-12954. https://doi.org/10.1029/96ja00611

Birn, J., Raeder, J., Wang, Y., Wolf, R., & Hesse, M. (2004). On the propagation of bubbles in the geomagnetic tail. *Annales Geophysicae*, *22*(5), 1773–1786. https://doi.org/10.5194/angeo-22-1773-2004

Birn, J., Thomsen, M., Borovsky, J., Reeves, G., McComas, D., Belian, R., & Hesse, M. (1998). Substorm electron injections: Geosynchronous observations and test particle simulations. *Journal of Geophysical Research*, *103*(A5), 9235–9248. https://doi.org/10.1029/97ja02635

Chen, Y., & Tóth, G. (2019). Gauss's law satisfying energy-conserving semi-implicit particle-in-cell method. *Journal of Computational Physics*, *386*, 632–652. https://doi.org/10.1016/j.jcp.2019.02.032

Chen, Y., Tóth, G., Cassak, P., Jia, X., Gombosi, T. I., Slavin, J., et al. (2017). Global three-dimensional simulation of earth's dayside reconnection using a two-way coupled magnetohydrodynamics with embedded particle-in-cell model: Initial results. *Journal of Geophysical Research*, *122*(10), 10318. https://doi.org/10.1002/2017JA024186

Chen, Y., Tóth, G., Hietala, H., Vines, S. K., Zou, Y., Nishimura, Y., et al. (2020). Magnetohydrodynamic with embedded particle-in-cell simulation of the geospace environment modeling dayside kinetic processes challenge event. *Earth and Space Science*, *7*(11), e2020EA001331. https://doi.org/10.1029/2020EA001331

Chen, Y., Tóth, G., Jia, X., Slavin, J. A., Sun, W., Markidis, S., et al. (2019). Studying dawn-dusk asymmetries of mercury's magnetotail using mhd-epic simulations. *Journal of Geophysical Research: Space Physics*, *124*(11), 8954–8973. https://doi.org/10.1029/2019ja026840

Chen, Y., Tóth, G., Zhou, H., & Wang, X. (2023). Fleks: A flexible particle-in-cell code for multi-scale plasma simulations. *Computer Physics Communications*, *287*, 108714. https://doi.org/10.1016/j.cpc.2023.108714

Daldorff, L. K. S., Tóth, G., Gombosi, T. I., Lapenta, G., Amaya, J., Markidis, S., & Brackbill, J. U. (2014). Two-way coupling of a global Hall magnetohydrodynamics model with a local implicit Particle-in-Cell model. *Journal of Computational Physics*, *268*, 236–254. https://doi.org/10.1016/j.jcp.2014.03.009

Daughton, W., Roytershteyn, V., Karimabadi, H., Yin, L., Albright, B., Bergen, B., & Bowers, K. (2011). Role of electron physics in the development of turbulent magnetic reconnection in collisionless plasmas. *Nature Physics*, *7*(7), 539–542. https://doi.org/10.1038/nphys1965

Eastwood, J., Goldman, M., Hietala, H., Newman, D., Mistry, R., & Lapenta, G. (2015). Ion reflection and acceleration near magnetotail dipolarization fronts associated with magnetic reconnection. *Journal of Geophysical Research: Space Physics*, *120*(1), 511–525. https://doi.org/10.1002/2014ja020516

Fu, H. S., Khotyaintsev, Y. V., André, M., & Vaivads, A. (2011). Fermi and betatron acceleration of suprathermal electrons behind dipolarization fronts. *Geophysical Research Letters*, *38*(16). https://doi.org/10.1029/2011gl048528

Fu, H. S., Khotyaintsev, Y. V., Vaivads, A., André, M., & Huang, S. (2012). Electric structure of dipolarization front at sub-proton scale. *Geophysical Research Letters*, *39*(6). https://doi.org/10.1029/2012gl051274

Gabrielse, C., Angelopoulos, V., Runov, A., & Turner, D. L. (2014). Statistical characteristics of particle injections throughout the equatorial magnetotail. *Journal of Geophysical Research: Space Physics*, *119*(4), 2512–2535. https://doi.org/10.1002/2013ja019638

Ge, Y., Raeder, J., Angelopoulos, V., Gilson, M., & Runov, A. (2011). Interaction of dipolarization fronts within multiple bursty bulk flows in global mhd simulations of a substorm on 27 February 2009. *Journal of Geophysical Research*, *116*(A5). https://doi.org/10.1029/2010ja015758

Gombosi, T. I., Chen, Y., Glocer, A., Huang, Z., Jia, X., Liemohn, M. W., et al. (2021). What sustained multi-disciplinary research can achieve: The space weather modeling framework. *Journal of Space Weather and Space Climate*, *11*, 42. https://doi.org/10.1051/swsc/2021020

Henderson, M., Reeves, G., & Murphree, J. (1998). Are north-south aligned auroral structures an ionospheric manifestation of bursty bulk flows? *Geophysical Research Letters*, *25*(19), 3737–3740. https://doi.org/10.1029/98gl02692

Hoshino, M. (2005). Electron surfing acceleration in magnetic reconnection. *Journal of Geophysical Research*, *110*(A10). https://doi.org/10.1029/2005ja011229

Huang, S., Fu, H., Yuan, Z., Zhou, M., Fu, S., Deng, X., et al. (2015). Electromagnetic energy conversion at dipolarization fronts: Multispacecraft results. *Journal of Geophysical Research: Space Physics*, *120*(6), 4496–4502. https://doi.org/10.1002/2015ja021083

Lapenta, G., Markidis, S., Divin, A., Goldman, M., & Newman, D. (2010). Scales of guide field reconnection at the hydrogen mass ratio. *Physics of Plasmas*, *17*(8), 082106. https://doi.org/10.1063/1.3467503

Li, C., Jia, X., Chen, Y., Toth, G., Zhou, H., Slavin, J. A., et al. (2023). Global hall MHD simulations of mercury's magnetopause dynamics and FTEs under different solar wind and IMF conditions. *Journal of Geophysical Research: Space Physics*, *128*(5), e2022JA031206. https://doi.org/10.1029/2022JA031206

Liu, C., Fu, H., Xu, Y., Cao, J., & Liu, W. (2017). Explaining the rolling-pin distribution of suprathermal electrons behind dipolarization fronts. *Geophysical Research Letters*, *44*(13), 6492–6499. https://doi.org/10.1002/2017gl074029

Liu, Y.-H., Birn, J., Daughton, W., Hesse, M., & Schindler, K. (2014). Onset of reconnection in the near magnetotail: Pic simulations. *Journal of Geophysical Research: Space Physics*, *119*(12), 9773–9789. https://doi.org/10.1002/2014ja020492

Lu, S., Angelopoulos, V., & Fu, H. (2016). Suprathermal particle energization in dipolarization fronts: Particle-in-cell simulations. *Journal of Geophysical Research: Space Physics*, *121*(10), 9483–9500. https://doi.org/10.1002/2016ja022815

Lyon, J., Fedder, J., & Mobarry, C. (2004). The Lyon-Fedder-Mobarry (LFM) global MHD magnetospheric simulation code. *Journal of Atmospheric and Solar-Terrestrial Physics*, *66*(15–16), 1333–1350. https://doi.org/10.1016/j.jastp.2004.03.020

Ma, Y., Russell, C. T., Toth, G., Chen, Y., Nagy, A. F., Harada, Y., et al. (2018). Reconnection in the martian magnetotail: Hall-MHD with embedded particle-in-cell simulations. *Journal of Geophysical Research: Space Physics*, *123*(5), 3742–3763. https://doi.org/10.1029/2017ja024729

Nakamura, R., Baumjohann, W., Klecker, B., Bogdanova, Y., Balogh, A., Rème, H., et al. (2002). Motion of the dipolarization front during a flow burst event observed by cluster. *Geophysical Research Letters*, *29*(20). https://doi.org/10.1029/2002gl015763

Nakamura, R., Baumjohann, W., Mouikis, C., Kistler, L., Runov, A., Volwerk, M., et al. (2004). Spatial scale of high-speed flows in the plasma sheet observed by cluster. *Geophysical Research Letters*, *31*(9). https://doi.org/10.1029/2004gl019558

Nakamura, R., Retinò, A., Baumjohann, W., Volwerk, M., Erkaev, N., Klecker, B., et al. (2009). Evolution of dipolarization in the near-earth current sheet induced by earthward rapid flux transport. *Annales Geophysicae*, *27*(4), 1743–1754. https://doi.org/10.5194/angeo-27-1743-2009

Øieroset, M., Lin, R., Phan, T., Larson, D., & Bale, S. (2002). Evidence for electron acceleration up to 300 k e v in the magnetic reconnection diffusion region of earth's magnetotail. *Physical Review Letters*, *89*(19), 195001. https://doi.org/10.1103/physrevlett.89.195001

Pollock, C., Moore, T., Jacques, A., Burch, J., Gliese, U., Saito, Y., et al. (2016). Fast plasma investigation for magnetospheric multiscale. *Space Science Reviews*, *199*(1–4), 331–406. https://doi.org/10.1007/s11214-016-0245-4

Powell, K., Roe, P., Linde, T., Gombosi, T., & De Zeeuw, D. L. (1999). A solution-adaptive upwind scheme for ideal magnetohydrodynamics. *Journal of Computational Physics*, *154*(2), 284–309. https://doi.org/10.1006/jcph.1999.6299

Pritchett, P. (2006). Relativistic electron production during driven magnetic reconnection. *Geophysical Research Letters*, *33*(13). https://doi.org/10.1029/2005gl025267

Raeder, J., Larson, D., Li, W., Kepko, E. L., & Fuller-Rowell, T. (2008). OpenGGCM simulations for the THEMIS mission. *Space Science Reviews*, *141*(1–4), 535–555. https://doi.org/10.1007/s11214-008-9421-5

Ridley, A., Gombosi, T., & Dezeeuw, D. (2004). Ionospheric control of the magnetosphere: Conductance. *Annales Geophysicae*, *22*(2), 567–584. https://doi.org/10.5194/angeo-22-567-2004

Runov, A., Angelopoulos, V., Gabrielse, C., Liu, J., Turner, D., & Zhou, X.-Z. (2015). Average thermodynamic and spectral properties of plasma in and around dipolarizing flux bundles. *Journal of Geophysical Research: Space Physics*, *120*(6), 4369–4383. https://doi.org/10.1002/2015ja021166

Runov, A., Angelopoulos, V., Sitnov, M., Sergeev, V., Bonnell, J., McFadden, J., et al. (2009). Themis observations of an earthward-propagating dipolarization front. *Geophysical Research Letters*, *36*(14). https://doi.org/10.1029/2009gl038980

Runov, A., Angelopoulos, V., & Zhou, X.-Z. (2012). Multipoint observations of dipolarization front formation by magnetotail reconnection. *Journal of Geophysical Research*, *117*(A5). https://doi.org/10.1029/2011ja017361

Sun, W., Turner, D. L., Zhang, Q., Wang, S., Egedal, J., Leonard, T., et al. (2022). Properties and acceleration mechanisms of electrons up to 200 kev associated with a flux rope pair and reconnection x-lines around it in earth's plasma sheet. *Journal of Geophysical Research: Space Physics*, *127*(12), e2022JA030721. https://doi.org/10.1029/2022ja030721

SWMF-Team. (2024). Space weather modeling framework [software]. https://clasp.engin.umich.edu/research/theory-computational-methods/space-weather-modeling-framework/swmf-downloadable-software/

Toffoletto, F., Sazykin, S., Spiro, R., & Wolf, R. (2003). Inner magnetospheric modeling with the Rice Convection Model. *Space Science Reviews*, *107*(1/2), 175–196. https://doi.org/10.1023/A:1025532008047

Tóth, G., Chen, Y., Gombosi, T. I., Cassak, P., Markidis, S., & Peng, B. (2017). Scaling the ion inertial length and its implications for modeling reconnection in global simulations. *Journal of Geophysical Research*, *122*(10), 10336. https://doi.org/10.1002/2017JA024189

Tóth, G., Jia, X., Markidis, S., Peng, B., Chen, Y., Daldorff, L., et al. (2016). Extended magnetohydrodynamics with embedded particle-in-cell simulation of Ganymede's magnetosphere. *Journal of Geophysical Research*, *121*(2), 1273–1293. https://doi.org/10.1002/2015JA021997

Tóth, G., Ma, Y. J., & Gombosi, T. I. (2008). Hall magnetohydrodynamics on block adaptive grids. *Journal of Computational Physics*, *227*(14), 6967–6984. https://doi.org/10.1016/j.jcp.2008.04.010

Tóth, G., van der Holst, B., Sokolov, I. V., Zeeuw, D. L. D., Gombosi, T. I., Fang, F., et al. (2012). Adaptive numerical algorithms in space weather modeling. *Journal of Computational Physics*, *231*(3), 870–903. https://doi.org/10.1016/j.jcp.2011.02.006

Wang, X. (2024). Mhd-aepic simulation for bursty bulk flows [dataset]. *University of Michigan - Deep Blue Data*. https://doi.org/10.7302/2yqp-7q96

Wang, X., Chen, Y., & Tóth, G. (2022a). Global magnetohydrodynamic magnetosphere simulation with an adaptively embedded particle-in-cell model. *Journal of Geophysical Research: Space Physics*, *127*(8), e2021JA030091. https://doi.org/10.1029/2021ja030091

Wang, X., Chen, Y., & Tóth, G. (2022b). Simulation of magnetospheric sawtooth oscillations: The role of kinetic reconnection in the magnetotail. *Geophysical Research Letters*, *49*(15), e2022GL099638. https://doi.org/10.1029/2022gl099638

Wiltberger, M., Merkin, V., Lyon, J., & Ohtani, S. (2015). High-resolution global magnetohydrodynamic simulation of bursty bulk flows. *Journal of Geophysical Research: Space Physics*, *120*(6), 4555–4566. https://doi.org/10.1002/2015ja021080

Wiltberger, M., Pulkkinen, T., Lyon, J., & Goodrich, C. (2000). MHD simulation of the magnetotail during the December 10, 1996, substorm. *Journal of Geophysical Research*, *105*(A12), 27649–27663. https://doi.org/10.1029/1999ja000251

Wolf, R. A., Harel, M., Spiro, R. W., Voigt, G., Reiff, P. H., & Chen, C. K. (1982). Computer simulation of inner magnetospheric dynamics for the magnetic storm of July 29, 1977. *Journal of Geophysical Research*, *87*(A8), 5949–5962. https://doi.org/10.1029/JA087iA08p05949

Xu, Y., Fu, H., Norgren, C., Toledo-Redondo, S., Liu, C., & Dong, X. (2019). Ionospheric cold ions detected by MMS behind dipolarization fronts. *Geophysical Research Letters*, *46*(14), 7883–7892. https://doi.org/10.1029/2019gl083885

Zhou, H., Tóth, G., Jia, X., & Chen, Y. (2020). Reconnection-driven dynamics at Ganymede's upstream magnetosphere: 3-d global hall MHD and MHD-epic simulations. *Journal of Geophysical Research: Space Physics*, *125*(8), e2020JA028162. https://doi.org/10.1029/2020ja028162

Zhou, H., Tóth, G., Jia, X., Chen, Y., & Markidis, S. (2019). Embedded kinetic simulation of Ganymede's magnetosphere: Improvements and inferences. *Journal of Geophysical Research: Space Physics*, *124*(7), 5441–5460. https://doi.org/10.1029/2019ja026643

Zhou, X.-Z., Angelopoulos, V., Sergeev, V., & Runov, A. (2010). Accelerated ions ahead of earthward propagating dipolarization fronts. *Journal of Geophysical Research*, *115*(A5). https://doi.org/10.1029/2010ja015481

Zhou, X.-Z., Angelopoulos, V., Sergeev, V., & Runov, A. (2011). On the nature of precursor flows upstream of advancing dipolarization fronts. *Journal of Geophysical Research*, *116*(A3). https://doi.org/10.1029/2010ja016165

Zhou, X.-Z., Pan, D.-X., Angelopoulos, V., Liu, J., Runov, A., Li, S.-S., et al. (2015). Ion acceleration and reflection on magnetotail anti-dipolarization fronts. *Geophysical Research Letters*, *42*(21), 9166–9175. https://doi.org/10.1002/2015gl065865

Zhou, X.-Z., Xu, Y., Runov, A., Liu, J., Artemyev, A. V., Angelopoulos, V., et al. (2019). On the origin of perpendicular ion anisotropy inside dipolarizing flux bundles. *Journal of Geophysical Research: Space Physics*, *124*(6), 4009–4021. https://doi.org/10.1029/2019ja026519